Manipulation of magnetic domain wall in magnetoelastic nanostripes

T. Mathurin[a], S. Giordano[a], Y. Dusch[a], N. Tiercelin[a], P. Pernod[a], V. Preobrazhenski[a]

a. Institut d'électronique, de Microélectronique et Nanotechnologie - IEMN UMR 8520, LIA LICS, Université Lille, CNRS, Centrale Lille, ISEN, Université Valenciennes, F-59000 Lille, France
theo.mathurin@gmail.com, stefano.giordano@iemn.univ-lille1.fr

Résumé :

Le mouvement de paroi de domaine est typiquement induit par des champs magnétiques externes ou des courants polarisés en spin. Cependant, des préoccupations concernant la consommation d'énergie de ces systèmes motive la recherche d'alternatives. Il en résulte un intérêt grandissant pour les différents couplages permettant d'utiliser des champs électriques plutôt que des courants pour déclencher le mouvement de paroi de domaine. Parmi les solutions potentielles, les matériaux magnétoélectriques passant par les contraintes mécaniques paraissent prometteurs. Dans ce contexte, la brisure de symétrie entre les états stables d'un nanoaimant autorise une implémentation plus simple du couplage mécanique. Ceci peut être obtenu grâce à un champ magnétique transverse. Dans un système à deux domaines, la contrainte provoque l'agrandissement de l'un par rapport à l'autre, ce qui cause le mouvement de la paroi de domaine. Ici, nous proposons une description des caractéristiques particulières du mouvement de paroi de domaine induit par contrainte mécanique. Dans nos simulations basées sur une procédure numérique ad-hoc, un nanoruban magnétoélastique présentant deux domaines est couplé à un substrat piézoélectrique PMN-PT de coupe <011>. Le design du profil de section du nanoruban permet de façonner la réponse statique et dynamique dans une certaine mesure. Du point de vue de la dynamique, le mouvement induit par les contraintes se distingue des régimes connus de mouvement du fait que la forme de paroi de domaine présente une excursion notable de l'aimanation hors du plan. Alors qu'on obtient des vitesses comparables à celles des autres techniques, cette approche est bien plus efficace en termes de consommation d'énergie.

Abstract :

The motion of domain walls is typically induced by external magnetic fields or spin-polarized currents. However, concerns about energy consumption of these systems motivates the search for alternatives. Thus, there is a growing interest in the different coupling allowing the use of electric fields instead of currents to trigger domain wall motion. Among these potential solutions, magnetoelectric materials mediated by mechanical stress appear promising. Since a uniform stress alone cannot induce unidirectional domain wall motion, the symmetry breaking of the stable states of a nanomagnet allows for a simpler implementation of the mechanical coupling. This can be achieved by a transverse magnetic field. In a two-domain system, the stress will then provoke the expansion of one of them at the expense of the other, which causes domain wall motion. Here, we propose a description of the peculiar characteristics of

domain wall motion induced by mechanical stress. In our simulations based on an ad-hoc procedure, a magnetoelastic nanostripe comprising two domains is coupled to a <011> cut PMN-PT piezoelectric substrate. The cross section design of the nanostripe allows the tailoring of the static and dynamic response to a certain extent. From a dynamical point of view, the motion induced by the stress differs from known motion regimes because the shape of the domain wall exhibits a remarkable out-of-plane excursion of the magnetization. While we get velocities comparable to those of other techniques, this approach is much more efficient in terms of energy consumption.

Mots clefs : stress-mediated coupling, magnetoelectric effect, magnetoelastic and piezoelectric materials, magnetic domain walls

1 Introduction

In macroscopic ferromagnetic materials, the magnetization is often not uniform, with the distribution such that the overall magnetization is zero. Regions of uniform magnetization are separated by localized structures called domain walls (DWs) within which the magnetization is strongly variable. Their manipulation is currently a subject of strong interest - especially in confined geometries such as nanowires, nanostripes and thin films - for both the search of fundamental insights and applications. The latters include for instance the storage [1, 2, 3, 4] and processing [5, 6, 7, 8] of information. DW motion is typically induced by external magnetic fields [9, 10, 11, 12] or spin-polarized currents[13, 14, 15, 16, 17, 18]. However, in order to reduce energy consumption in these systems, there is a considerable interest in the use of electric fields, instead of electric currents. One way of implementing this magnetoelectric coupling is to use mechanical stress as an intermediate, for example by coupling a piezoelectric substrate with a magnetoelastic material. However, a uniform stress does not directly induce a unidirectional DW motion in head-to-head (180°) structures. For this reason, the mechanical coupling has been proposed in complex heterostructures of rather convoluted realization and operation. For instance, a localized non-uniform mechanical stress has been exploited to move a DW in a nanowire sandwiched between a substrate and a multi-contacted piezoelectric layer [19, 20]. A recent application of this principle has been exploited to produce the rotation of a DW in a ferromagnetic ring fabricated on a piezoelectric substrate [21, 22]. Also, the dynamics of a current- or field-induced DW can be piezoelectrically controlled through a strain-mediated magnetic anisotropy [24, 23, 25, 26]. Moreover, the magnetic DW motion can be caused by pinning onto moving ferroelectric DWs [27, 28]. The strain-mediated electric control of domain structures can be obtained for domain wall between orthogonal states (90°) in cubic ferromagnets without using an external magnetic field [29]. A promising alternative is based on the symmetry breaking of the two opposite stable magnetization states arising from the uniaxial anisotropy of unidimensional ferromagnets. Basically, this can be realized through a static magnetic field, *e.g.* generated by permanent magnets, which is perpendicularly applied to the ferromagnetic easy axis. The consequent tilting of the states allows for their manipulation by way of uniform mechanical actions. This mechanism has been used to mechanically switch the magnetization of magnetoelastic particles [30, 31, 32, 33, 34, 35, 36, 37, 38] or to induce DW motion with uniform stresses [39, 40, 41]. While the magneto-electro-elastic coupling in composite systems has been largely studied both experimentally [42] and theoretically in the linear [43] and nonlinear [44, 45] regimes, the exploitation of the magnetization dynamics in multi-layered systems is a recent application with important implications in memories, spintronics and new paradigms of information processing.

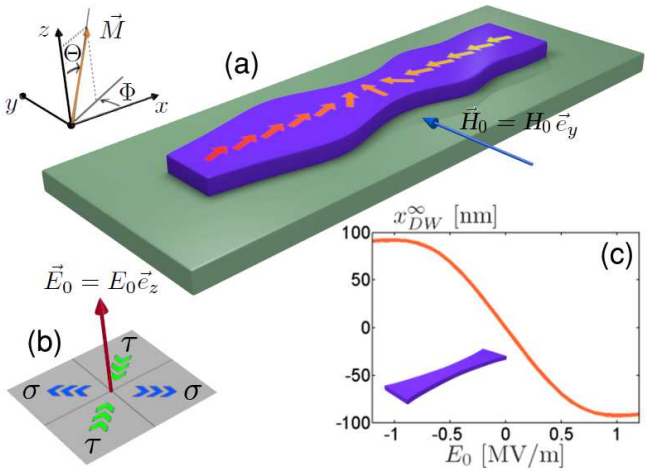

FIGURE 1 – (a) Sketch of the system constituted by a magnetoelastic nanostripe deposited on a piezoelectric substrate. The magnetization vector $\vec{M}$ is described by angles Φ and Θ and the nanostripe easy-axis is along x. A DW is thus created between two states tilted by the magnetic field $\vec{H}_0$. (b) Stress components $\sigma > 0$ and $\tau < 0$ generated by the electric field $\vec{E}_0 = E_0\vec{e}_z$ with $E_0 > 0$ (if $E_0 < 0$, then $\sigma < 0$ and $\tau > 0$). (c) DW equilibrium position versus electric field in a nanostripe with parabolic shape.

Here, we investigate the distinctive DW dynamics induced in an amorphous magnetoelastic nanostripe by the combination of a tilting magnetic field $\vec{H}_0$ and a uniform stress generated by a piezoelectric substrate (see Fig.1a). The applied stress considered is composed of uniform orthogonal tensile and compressive components (σ and τ in Fig.1b), and is controlled by an electric field $\vec{E}_0$ via the piezoelectric effect. We provide evidence that the DW velocity is of the same order of magnitude as that of field- or current-induced motion, while the energy consumption is between one and two orders of magnitude smaller. Tailoring of the static and dynamic responses is possible through the engineering of the cross-section. We will discuss the parabolic and constant section profiles, leading to a precise position and velocity control, respectively. In particular, the parabolic profile yields a reversible behavior with a one-to-one correspondence between applied stress (or electric field) and DW position (see Fig.1c). It is worth noticing that contrary to the well-known steady-state Walker DW dynamics, where the magnetization is always contained in a given plane [46], we observe here local out-of-plane excursions of the magnetization vector during its evolution.

We briefly describe the physical principle exploited in the proposed system. We take into consideration the magnetoelastic layer placed on the piezoelectric substrate, as represented in Fig.1a. The stripe shows a uniaxial anisotropy, which tends to align the magnetization along x-axis (without any preference between positive and negative directions). We propose to apply a magnetic field along the y-axis. From the technological point of view, the system can be simply placed in the air gap of a surrounding magnetic circuit, which includes an arrangement of permanent magnets. Given the lengthscales involved it is rather certain that the homogeneity of the magnetic field generated by such a device would be secured over the whole nanostripe. In the case of applications for which integration concerns are relevant, macroscopic magnets may generate more uniform fields in a given region and can be adopted without limiting the integration density on a given substrate. Therefore, all magnetoelastic nanostripes would be subjected to the same magnetic bias. Anyway, the competition between the magnetic anisotropy and the applied magnetic field generates two energetically equivalent stable orientations for the nanostripe magnetization. We can therefore consider a domain wall between two domains characterized by these

two magnetization states, as shown by the arrows distribution within the nanostripe in Fig.1a. To induce the domain wall motion, we take advantage of the magnetostriction of the nanostripe, coupled with the piezoelectric substrate. Indeed, in an arbitrarily strained magnetostrictive layer, the magnetization tends to be aligned with the direction of the larger geometrical elongation. We can exploit this property through a varying (positive or negative) electric field applied to the piezoelectric substrate, which generates tensile and compressive stress components, as shown in Fig.1b. Consequently, it is not difficult to recognize that a positive electric field leads to a leftward motion of the domain wall, whereas a negative electric field leads to its rightward motion. This is the principle of operation of the proposed system, and it can be exploited with different profiles of the ferromagnetic nanostripe for obtaining specific dynamic behaviors.

The paper is structured as follows. In Section 2 we describe the model adopted to analyse the dynamics of the system. In Section 3 we present the results based on the numerical solution of the equations obtained in Section 2. Finally, in Section 4 we discuss the conclusions and some perspectives.

2 The model

We consider the systam described in Fig.1 and, to model its dynamics, we assume that the magnetization $\vec{M}$ depends only on x and t. This hypothesis is reasonable if the thickness and width of the nanomagnet are small compared to its length. We remark that this assumption has been largely used in the past to study the motion of a domain wall induced by an external magnetic field, yielding results in good agreement with experiments [46]. Therefore, we can write $\vec{M} = M_s\vec{\gamma}$, where M_s is the magnetization at saturation and $\vec{\gamma} = (\cos\Phi\sin\Theta, \sin\Phi\sin\Theta, \cos\Theta)$ is a unit vector with $\Phi = \Phi(x,t)$ and $\Theta = \Theta(x,t)$ (see Fig.1a). The total energy density

$$u = u_{an} + u_{Ze} + u_{de} + u_{ex} + u_{me} \tag{1}$$

within the nanostripe is composed of the following terms. The uniaxial anisotropy along x is given by

$$u_{an} = -K_u\gamma_x^2, \tag{2}$$

where K_u represents the anisotropy coefficient. On the other hand, the Zeeman contribution corresponds to

$$u_{Ze} = -\mu_0 M_S H_0 \gamma_y, \tag{3}$$

where μ_0 is the permeability of free space and H_0 is the intensity of the magnetic field applied along the y-axis. Similarly, the demagnetization energy density is given by

$$u_{de} = -\frac{1}{2}\mu_0 M_s \vec{H}_d \cdot \vec{\gamma}, \tag{4}$$

in which $\vec{H}_d$ is the demagnetization field defined as

$$\vec{H}_d(\vec{r}) = M_S \int_\Omega \hat{N}\left(\vec{r},\vec{r}_0\right)\vec{\gamma}\left(\vec{r}_0\right)\mathrm{d}\vec{r}_0, \tag{5}$$

where Ω is the whole magnetoelastic region defined by $-\frac{L}{2} \leq x \leq +\frac{L}{2}$, $-\frac{\ell(x)}{2} \leq y \leq +\frac{\ell(x)}{2}$, and $-\frac{h}{2} \leq z \leq +\frac{h}{2}$. The quantity $\hat{N}$ represents the demagnetization tensor [39, 40]

$$\hat{N}\left(\vec{r},\vec{r}_0\right) = \frac{1}{4\pi}\left[\frac{3\left(\vec{r}-\vec{r}_0\right)\otimes\left(\vec{r}-\vec{r}_0\right)}{\|\vec{r}-\vec{r}_0\|^5} - \frac{\hat{I}}{\|\vec{r}-\vec{r}_0\|^3}\right] \tag{6}$$

where $\vec{a}\otimes\vec{b}$ represents the tensor product between two vectors $\vec{a}$ and $\vec{b}$, *i.e.* $\left(\vec{a}\otimes\vec{b}\right)_{ij} = a_i b_j$, and $\hat{I}$ is the identity operator. The exchange energy density can be written as

$$u_{ex} = A\left(\mathrm{d}\vec{\gamma}/\mathrm{d}x\right)^2, \tag{7}$$

where A is the exchange coefficient. The general form of the magnetoelastic energy density is

$$u_{me} = -T_{ij}\epsilon^{\mu}_{ij}, \tag{8}$$

where T_{ij} is the local Cauchy stress tensor and $\epsilon^{\mu}_{ij}\left(\vec{\gamma}\right)$ is the magnetostrictive strain. Its mathematical expression is $\epsilon^{\mu}_{ij} = \frac{\lambda_S}{2}(3\gamma_i\gamma_j - \delta_{ij})$, where λ_S is the magnetostriction coefficient. The elastic and magnetoelastic properties of the ferromagnetic stripe are assumed to be isotropic (amorphous ferromagnets). With the geometry of Fig.1, we obtain

$$u_{me} = -\frac{3}{4}\lambda_S\left[(\tau+\sigma)\left(\gamma_x^2+\gamma_y^2\right) + 2(\tau-\sigma)\gamma_x\gamma_y\right], \tag{9}$$

where τ and σ are the stress components along $\vec{e}_\tau = (\vec{e}_x+\vec{e}_y)/\sqrt{2}$ and $\vec{e}_\sigma = (\vec{e}_y-\vec{e}_x)/\sqrt{2}$, respectively ($\vec{e}_i$ is the unit vector along the i-axis). Their values are defined by $\tau = 2\mu E_0(d_{31}+\nu d_{32})/(1-\nu)$ and $\sigma = 2\mu E_0(d_{32}+\nu d_{31})/(1-\nu)$. Here, μ and ν are the shear modulus and the Poisson ratio of the magnetoelastic nanostripe and d_{31} and d_{32} are the piezoelectric coefficients of the substrate. They control the strains $\varepsilon_\tau = d_{31}E_0$ and $\varepsilon_\sigma = d_{32}E_0$, along $\vec{e}_\tau$ and $\vec{e}_\sigma$ respectively, transmitted without loss to the nanostripe. Although the spatial uniformity of stresses τ and σ and of the magnetic field $\vec{H}_0$ may not be rigorously fulfilled in real structures because of experimental constraints, we suppose to deal here with uniform fields in order to shed light on the peculiar physics generated by the coexistence of τ, σ and $\vec{H}_0$. Presumably, the resulting behavior would be only slightly altered as the model is made more realistic. For the same reason, the edge roughness, possibly generating potential wells for the DW [47], is also here neglected. Because the roughness creates barriers with metastable states, the motion can be hampered and the actual velocity may depart from predictions. Typically, this equates to the emergence of a *creep regime* at low fields [47]. However, there is a given thresholds (depinning) for the fields beyond which the domain wall behavior will approach the usual *flow regime* predicted theoretically.

To sum up, the total energy density of the system is

$$\begin{aligned} u &= -K_u\gamma_x^2 - \mu_0 M_S H_0\gamma_y - \frac{1}{2}\mu_0 M_s\vec{H}_d\cdot\vec{\gamma} + A\left(\mathrm{d}\vec{\gamma}/\mathrm{d}x\right)^2 \\ &\quad -\frac{3}{4}\lambda_S\left[(\tau+\sigma)\left(\gamma_x^2+\gamma_y^2\right) + 2(\tau-\sigma)\gamma_x\gamma_y\right], \end{aligned} \tag{10}$$

and the total energy U can be finally calculated by integrating Eq.(10) over the ferromagnetic region Ω

$$\begin{aligned} U &= \int_\Omega u dv \\ &= \int_{-L/2}^{+L/2} h\ell(x) \Big[-K_u\gamma_x^2 - \mu_0 M_S H_0 \gamma_y + A\left(\mathrm{d}\vec{\gamma}/\mathrm{d}x\right)^2 - \frac{3}{4}\lambda_S(\tau+\sigma)\left(\gamma_x^2+\gamma_y^2\right) \\ &\quad -\frac{3}{2}\lambda_S(\tau-\sigma)\gamma_x\gamma_y \Big] \mathrm{d}x - \frac{1}{2}\mu_0 M_S^2 \int_\Omega\int_\Omega \vec{\gamma}\left(\vec{r}\right)\cdot\hat{N}\left(\vec{r},\vec{r_0}\right)\vec{\gamma}\left(\vec{r_0}\right)\mathrm{d}\vec{r_0}\mathrm{d}\vec{r}, \end{aligned} \tag{11}$$

where the demagnetization tensor $\hat{N}$ is defined in Eq.(6). The minimization of the functional U defined in Eq.(11) can be performed as follows : $\min_{\vec{\gamma}} U'(\vec{\gamma})$, where

$$U'(\vec{\gamma}) = U(\vec{\gamma}) + \int_{-L/2}^{+L/2} \lambda(x)\left(\vec{\gamma}\cdot\vec{\gamma}-1\right)\mathrm{d}v, \tag{12}$$

and $\lambda = \lambda(x)$ is a Lagrange multiplier introduced to fix the norm of the unit vector $\vec{\gamma}$. The application of the variational calculus to this minimization problem entails the solution of the following equation

$$\frac{\mathrm{d}}{\mathrm{d}\alpha} U'\left[\vec{\gamma}(x) + \alpha\vec{h}(x)\right]\Big|_{\alpha=0} = 0 \qquad \forall\, \vec{h}(x). \tag{13}$$

The development of this derivative, not reported here for the sake of brevity, yields the static or equilibrium equation $\vec{\gamma}\wedge\vec{H}_{eff} = 0$, where the effective field $\vec{H}_{eff}$ is given by

$$\begin{aligned} \vec{H}_{eff} &= H_0\vec{e}_y + \left\langle\vec{H}_d\right\rangle + \frac{2K_u\gamma_x\vec{e}_x}{\mu_0 M_S} + \frac{2A}{\mu_0 M_S \ell}\frac{\partial}{\partial x}\left(\ell\frac{\partial\vec{\gamma}}{\partial x}\right) \\ &\quad + \frac{3\sqrt{2}\lambda_S}{2\mu_0 M_S}\left[(\gamma_x+\gamma_y)\tau\vec{e}_\tau - (\gamma_x-\gamma_y)\sigma\vec{e}_\sigma\right], \end{aligned} \tag{14}$$

and $\ell(x)$ is the profile of the variable section. Here, $\left\langle\vec{H}_d\right\rangle$ represents the average value of $\vec{H}_d$ on the (y,z) cross-section of the nanostripe

$$\langle\vec{H}_d\rangle(x) = \frac{1}{h\ell(x)} \int_{-\frac{\ell(x)}{2}}^{+\frac{\ell(x)}{2}} \int_{-\frac{h}{2}}^{+\frac{h}{2}} \vec{H}_d(\vec{r})\mathrm{d}z\mathrm{d}y. \tag{15}$$

The effective field $\vec{H}_{eff}$ can now be inserted into the Landau-Lifshitz-Gilbert (LLG) equation

$$\frac{\mathrm{d}\vec{\gamma}}{\mathrm{d}t} = -\mu_0\mathcal{G}\vec{\gamma}\wedge\vec{H}_{eff} + \alpha\vec{\gamma}\wedge\frac{\mathrm{d}\vec{\gamma}}{\mathrm{d}t}, \tag{16}$$

describing the magnetization dynamics [48, 49]. We eventually obtain its explicit form

$$\begin{cases} \dot{\Phi} &= \mathsf{G}(\alpha\mathsf{r}-\mathsf{s})/\sin\Theta, \\ \dot{\Theta} &= \mathsf{G}\left(\alpha\mathsf{s}+\mathsf{r}\right), \end{cases} \tag{17}$$

where α is the damping coefficient, $\mathsf{G} = \mu_0\mathcal{G}/(1+\alpha^2)$, $\mathcal{G} = 1.76\times10^{11}\mathrm{rad\ s^{-1}T^{-1}}$ is the electron

gyromagnetic ratio, and r and s follow

$$\begin{aligned}
\mathsf{r} &= -\sin\Phi\,\langle H_{dx}\rangle + \cos\Phi\,\langle H_{dy}\rangle + \cos\Phi H_0 - \frac{2K_u}{\mu_0 M_S}\cos\Phi\sin\Phi\sin\Theta \\
&\quad + \frac{3}{2}\frac{\lambda_S}{\mu_0 M_S}(\tau-\sigma)\cos(2\Phi)\sin\Theta + \frac{2A}{\mu_0 M_S}\left(\frac{\ell'}{\ell}\Phi'\sin\Theta + 2\Phi'\Theta'\cos\Theta + \Phi''\sin\Theta\right), \quad (18)\\
\mathsf{s} &= \cos\Phi\cos\Theta\,\langle H_{dx}\rangle + \sin\Phi\cos\Theta\,\langle H_{dy}\rangle - \sin\Theta\,\langle H_{dz}\rangle + \sin\Phi\cos\Theta H_0 \\
&\quad + \frac{2K_u}{\mu_0 M_S}\cos^2\Phi\sin\Theta\cos\Theta + \frac{3}{2}\frac{\lambda_S}{\mu_0 M_S}\cos\Theta\sin\Theta\left[(\tau+\sigma) + \sin(2\Phi)(\tau-\sigma)\right] \\
&\quad + \frac{2A}{\mu_0 M_S}\left(\frac{\ell'}{\ell}\Theta' + \Theta'' - \Phi'^2\cos\Theta\sin\Theta\right). \quad (19)
\end{aligned}$$

Here, $\dot{f} \equiv \partial f/\partial t$ and $f' \equiv \partial f/\partial x$. Since $\left\langle \vec{H}_d \right\rangle$ is given by an integral expression depending on Θ and Φ (see Eqs.(5) and (15)), Eq.(17), combined with Eqs.(18) and (19), represents a system of two strongly non-linear partial integro-differential equations. To solve it, we developed an *ad hoc* numerical procedure based on an implicit nonlinear finite difference scheme combined with a precise calculation of the actual demagnetization field [40]. This methodology has been successfully tested against the exact Walker solution, describing the dynamics of a DW driven by a magnetic field [46]. Moreover, all solutions have been validated by testing their stability to large variations of the time step Δt and the discretization interval Δx. Of course, the analysis of the system proposed in the present paper could be performed with standard micromagnetic simulations. However, the numerical solution of our equations is less costly from the computational point of view and the discussed model provides a deeper understanding of the underlying physics.

3 Results

We present here the results concerning the dynamics of the system represented in Fig.1, obtained through the solution of Eqs.(17), (18) and (19) introduced in previous section. A $TbCo_2$/FeCo multilayered nanostripe with $M_s = 64\times10^4$A/m, $A = 9\times10^{-12}$J/m, $\mu = 80$GPa, $\nu = 0.25$, $\lambda_S = 2\times10^{-4}$ is the representative nanomagnet [39]. We use $K_u = 37.5\times10^3$J/m^3, $H_0 = 20\times10^3$A/m and $0.06 \le \alpha \le 0.12$, which are reasonable values in real systems. We also adopt the piezoelectric PMN-PT ceramic with $d_{32} = 600$pC/N and $d_{31} = -1900$pC/N [50].

We first discuss a parabola shaped nanostripe with thickness $h = 10$nm and $\ell(x) = a + 4\frac{b-a}{L^2}x^2$, where $a = \ell(0) = 40$nm (central width), $b = \ell(\pm L/2) = 70$nm (width at extremities) and $L = 400$nm (see Fig.2a). If $\vec{H}_0 = 0$ and $\vec{E}_0 = 0$, we consider a Néel DW at $x = 0$, between two domains of opposite magnetization (initial metastable condition). If $\vec{H}_0 \neq 0$ the states are tilted but still have the same energy, keeping the DW at $x = 0$. This equilibrium configuration is found with a nonlinear relaxation method applied to the equations $\mathsf{r} = 0$ and $\mathsf{s} = 0$ [39, 40], and is taken as initial condition to analyze the dynamics through Eq.(17). Indeed, when $\vec{E}_0 \neq 0$ is applied, the DW moves so as to reduce the size of the domain with higher energy density. By virtue of the adopted geometry with variable section, the DW reaches a final equilibrium position $x_{DW}^{\infty} = \lim_{t\to\infty} x_{DW}(t)$ depending on the strength of E_0 (see Fig.1c). There is in fact an exchange energy cost to increase its surface [39, 40]. The DW position can thus be unequivocally controlled and is symmetric for opposite values of E_0 (see again Fig.1c).

Contrary to the static response, the dynamics described by $\Phi = \Phi(x,t)$ and $\Theta = \Theta(x,t)$ (see Fig.2b), and $x_{DW}(t)$ (see Fig.2c) exhibits a remarkable asymmetry between $E_0 > 0$ and $E_0 < 0$. This intriguing

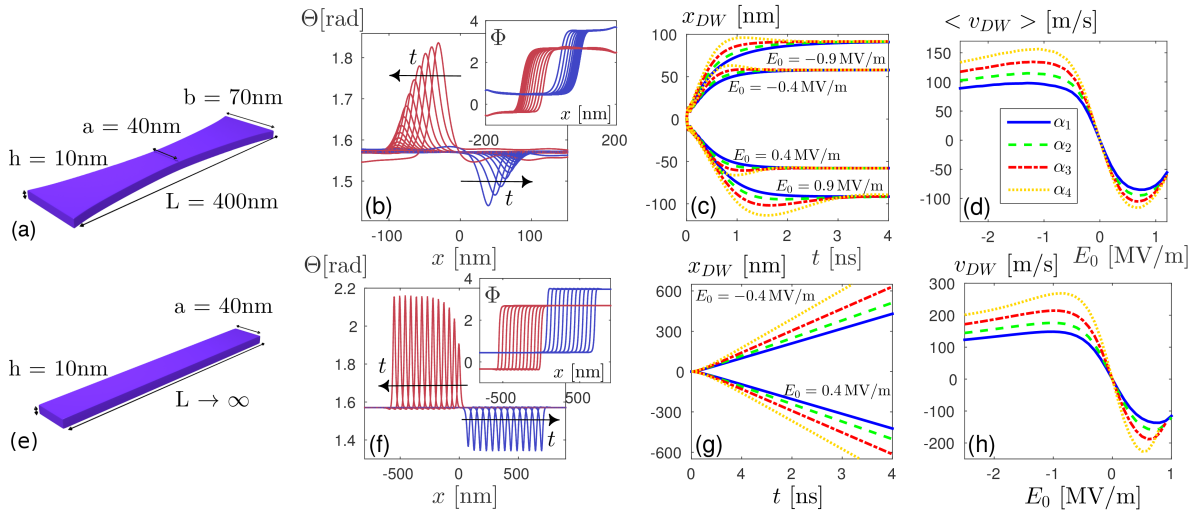

FIGURE 2 – Dynamics of the magnetic DW in the nanostripe with parabolic (a) and constant (e) section. (b,f) Evolution of the magnetization angles $\Theta(x,t)$ and $\Phi(x,t)$ (inset) obtained with $E_0 = \pm 0.8$MV/m and the damping parameter $\alpha = 0.1$ (angles versus x at different times t). If $E_0 > 0$, the DW moves to the left ($x < 0$), and if $E_0 < 0$, the DW moves to the right ($x > 0$). (c,g) Time evolution of x_{DW} for $\alpha_1 = 0.12$, $\alpha_2 = 0.1$, $\alpha_3 = 0.08$ and $\alpha_4 = 0.06$ and for the indicated values of E_0. (d,h) Asymmetric behavior of the DW velocity (average value $\langle v_{DW} \rangle$ for the parabolic nanostripe and steady-state value v_{DW} for the uniform nanostripe) versus electric field E_0 for the above values of α.

behavior is caused by the disparity $d_{32} \neq -d_{31}$. Indeed, σ and τ fulfil the relation $|\tau| > |\sigma|$ (and they are always of opposite sign). It means that if $E_0 > 0$, the DW moves to the left ($x < 0$) with a compression $|\tau|$ larger than the tension σ ; conversely, if $E_0 < 0$, the DW moves to the right ($x > 0$) with a tension τ larger than the compression $|\sigma|$. Since a compression induces a *planar anisotropy* from the magnetic point of view (perpendicularly to its direction) and a traction induces an *axial anisotropy* for the magnetization (along its direction), the motions to the left and to the right are not dynamically equivalent. They are so only if $d_{32} = -d_{31}$, when the identity $\tau = -\sigma$ is verified. In both directions of motion, unusual out-of plane excursions appear locally. When the compression is larger than the tension ($E_0 > 0$), the prevailing planar anisotropy induces out-of-plane excursions with considerable deviation of Θ from $\pi/2$ (see Fig.2a, $x < 0$), and the DW propagation is sensibly hindered [51]. On the other hand, when the tension is larger than the compression ($E_0 < 0$), the out-of-plane excursions are comparatively reduced (see Fig.2a, $x > 0$), and the DW motion is facilitated. As shown in Figs.2d, this phenomenon is more intense for large values of $|E_0|$. In Fig.2d, the quantity $\langle v_{DW} \rangle$ is defined as the average velocity over the path from the origin to the position $\frac{2}{3}x_{DW}^{\infty}$. While for $E_0 < 0$, with increasing $|E_0|$ we observe a maximum of $\langle v_{DW} \rangle$ and a following slight velocity decrease, for $E_0 > 0$ increasing values of E_0 lead to a minimum of $\langle v_{DW} \rangle$ immediately followed by a strong velocity reduction. This is consistent with the previous interpretation based on the magnetic planar and axial anisotropy. Noteworthy, for $|E_0| < 0.6$MV/m, we have a quite linear and symmetric response, a convenient feature for technological applications. This point is substantiated by calculating the energy consumption for moving the DW from $x_{DW}^{\infty}(-E_0)$ to $x_{DW}^{\infty}(+E_0)$. The magnetic dissipation for the case with $E_0 = 0.4$MV/m and $x_{DW}^{\infty} = \pm 60$nm corresponds to $E_m = 10^{-3}$fJ. Moreover, if we consider a cubic piezoelectric substrate of side d=800nm with relative permittivity $\varepsilon_r = 3500$, the electric energy consumed is $E_e = CV^2 = \varepsilon_0 \varepsilon_r d^3 E_0^2$ (where $C = \varepsilon_0 \varepsilon_r d$ and $V = E_0 d$). With $E_0 = 0.4$MV/m, we obtain $E_e = 2.5$fJ $\gg E_m$ for a DW displacement of 120nm for this geometry. If permanent magnets generate $\vec{H}_0$ [52], they do not dissipate

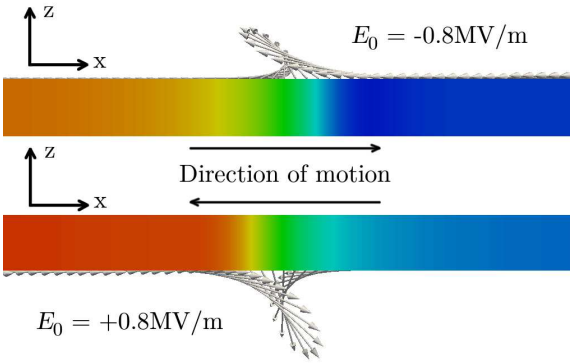

FIGURE 3 – Representations of the domain wall configuration in motion within the nanostripe with constant section. We show two different cases driven by negative and positive electric fields, corresponding to axial and planar effective magnetic anisotropy, respectively. We observe that the out-of-plane behavior is more pronounced for positive electric fields (planar anisotropy).

energy. To draw a comparison, the energy consumption of 200fJ has been reported to propagate a DW for a distance of 500nm through spin-polarized currents [18, 22]. Then, in the latter case the dissipation is about 20 times higher.

From a fundamental perspective, our results for the parabolic profile revealed a specific magnetic configuration with an out-of-plane excursion ($\Theta \neq \pi/2$) in proximity to the DW. In order to further investigate this point, we analyzed the DW propagation in a constant-section infinitely-long nanostripe (see Fig.2e), and we confirmed the existence of an unusual out-of-plane excursion. This dynamics is therefore substantially richer than the classical Walker propagation [46]. We observe the existence of a rapidly reached steady-state regime, characterized by $\Phi(x,t) = \Phi_0(x - v_{DW}t)$ and $\Theta(x,t) = \Theta_0(x - v_{DW}t)$ (see Fig.2f), where Φ_0 and Θ_0 represent the stationary shapes. The corresponding uniformity of the motion is shown in Fig.2g, the steady-state velocity v_{DW} being plotted versus the applied field E_0 in Fig.2h. In particular, Fig.2h shows that the constant section nanostripe exhibits the same asymmetric velocity behavior, already observed and analyzed for the parabolic nanostripe. This configuration allows the control of the DW velocity with the applied electric field. The behavior of the out-of-plane excursion can be observed in Figs.3 and 4. In Fig.3 we show the shape of the domain wall for two opposite values of the electric field. When we apply a positive field, the compressive in-plane strain is larger than the tensile one and this configuration creates a planar magnetoelastic anisotropy in a ferromagnetic film with positive magnetoelastic coefficient [51]. Such anisotropy favors a large perpendicular-to-plane orientation of the magnetization. On the contrary, a negative electric field induces a compressive strain larger than the tensile one, creating an in-plane easy axis of magnetization, corresponding to smaller of the out-of-plane excursions. This explains the asymmetry of the DW dynamics with positive and negative electric field. The out-of-plane excursions are more pronounced for large values of $|E_0|$, as shown in Fig.4 where the DW shape is represented for two different values of the electric field. We observe the peculiar form of the domain wall shape, characteristic of the magnetoelastic nanostripe and very different from the well-known Néel or Bloch walls.

Further enhancement of magnetic DW dynamics is possible by optimizing the tilting magnetic field $\vec{H}_0$. We show in Fig.5 the DW velocity versus the intensity H_0 in the constant section nanostripe for the same values of α adopted in Fig.2 and for three different values of E_0. We deduce that our mechanically induced steady-state regime yields propagation velocities as high as 500m/s, which are comparable to

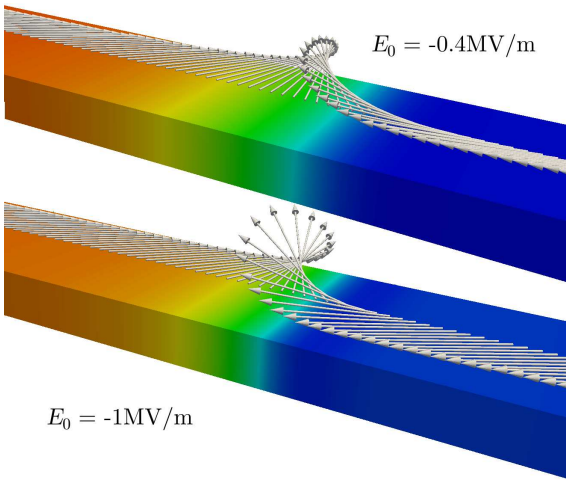

FIGURE 4 – Perspective representations of the domain wall configuration in motion within the nanostripe with constant section. We show two different cases driven by two different electric fields. We observe that the out-of-plane behavior is more pronounced for higher electric fields.

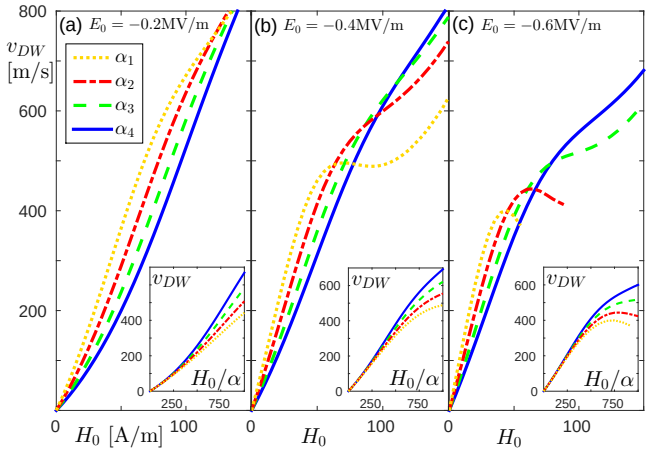

FIGURE 5 – Velocity of the DW in a constant-section infinitely-long nanostripe in terms of H_0 and α for $E_0 = -0.2$MV/m (a), $E_0 = -0.4$MV/m (b), and $E_0 = -0.6$MV/m (c). In the insets the collapse of the linear regime obtained by plotting v_{DW} versus H_0/α is shown. In all panels we used the same values of α introduced in Fig.2.

those obtained by current-driven DW motion [17, 18]. In the classical field-induced Walker propagation the dependence of the DW velocity on H_0 and α is mediated by the single variable H_0/α [46]. Hence, we plot v_{DW} versus the ratio H_0/α in the insets of Fig.5. We observe that the curves corresponding to different α collapse to a single universal response in the linear region. We also note that $\partial v_{DW}/\partial\rho$ (for low values of $\rho = H_0/\alpha$) is an increasing function of E_0, as expected. However, for higher values of the magnetic field, v_{DW} depends on both H_0/α and α, proving once again the essential difference between the mechanically-induced and the field-induced DW motion.

Finally, in order to validate the approximation adopted in our model, namely the consideration of the magnetization as a function of x and t only, we compared the solutions obtained with Eqs.(17), (18) and (19) with micromagnetic simulations performed within the NMAG environment. In any case, the relative error between the two techniques is found as small as 10%.

4 Conclusions

To conclude, we numerically demonstrated that the mechanical manipulation of DWs in magnetoelastic nanostripes can be simply achieved through uniform stresses if we break the symmetry of the states. The resulting moving magnetic structure, characterized by very-low energy dissipation and competitive velocities, is fundamentally different from usual DW in nanostripes being characterized by specific out-of-plane phenomena. The tailoring of the variable nanostripe section allows one to precisely design static and dynamic features. For instance, the applied electric field may control the DW position in parabolic nanostripes or the DW velocity in uniform nanostripes. Further, complex profiles $\ell(x)$ with two or more minima can be envisaged to realize hysteretic bistable or multi-stable systems. The DW motion driven by uniform mechanical stress thus deserves experimental investigation for both fundamental physics and applications.

Références

[1] S. S. Parkin, M. Hayashi, and L. Thomas, Science **320**, 190 (2008).

[2] J. H. Franken, H. J. M. Swagten, and B. Koopmans, Nat. Nanotechnol. 7, 499 (2012).

[3] S. Parkin and S.-H. Yang, Nat. Nanotechnol. **10**, 195 (2015).

[4] Y. P. Ivanov, A. Chuvilin, S. Lopatin, and J. Kosel, ACS Nano, **10**, 5326 (2016).

[5] D. A. Allwood, G. Xiong, C. Faulkner, D. Atkinson, D. Petit, and R. P. Cowburn, Science, **309**, 1688 (2005).

[6] B. Behin-Aein, D. Datta, S. Salahuddin, and S. Datta, Nat. Nanotechnol. **5**, 266 (2010).

[7] N. Locatelli, V. Cros, and J. Grollier, Nature Mater. **13**, 11 (2014).

[8] S. Lequeux, J. Sampaio, V. Cros, K. Yakushiji, A. Fukushima, R. Matsumoto, H. Kubota, S. Yuasa, J. Grollier, Sci. Rep. **6**, 31510 (2016).

[9] T. Ono, H. Miyajima, K. Shigeto, K. Mibu, N. Hosoito, and T. Shinjo, Science **284**, 468 (1999).

[10] D. Atkinson, D. A. Allwood, G. Xiong, M. D. Cooke, C. C. Faulkner, and R. P. Cowburn, Nature Mater. **2**, 85 (2003).

[11] Y. Nakatani, A. Thiaville, J. Miltat, Nat. Mater., **2**, 521 (2003).

[12] G. S. D. Beach, C. Nistor, C. Knutson, M. Tsoi, and J. L. Erskine, Nature Mater. **4**, 741 (2005).

[13] M. Kläui, C. A. F. Vaz, J. A. C. Bland, W. Wernsdorfer, G. Faini, E. Cambril, L. J. Heyderman, F. Nolting, U. Ru ?diger, Phys. Rev. Lett. **94**, 106601 (2005).

[14] M. Hayashi, L. Thomas, C. Rettner, R. Moriya, Y. B. Bazaliy, and S. S. P. Parkin, Phys. Rev. Lett. **98**, 037204 (2007).

[15] D. Ravelosona, S. Mangin, J. A. Katine, E. E. Fullerton, and B. D. Terris, Appl. Phys. Lett. **90**, 072508 (2007).

[16] A. V. Khvalkovskiy, V. Cros, D. Apalkov, V. Nikitin, M. Krounbi, K. A. Zvezdin, A. Anane, J. Grollier, and A. Fert, Phys. Rev. B **87**, 020402 (2013).

[17] S.-H. Yang, K.-S. Ryu, S. Parkin, Nat. Nanotechnol. **10**, 221 (2015).

[18] P. J. Metaxas, J. Sampaio, A. Chanthbouala, R. Matsumoto, A. Anane, A. Fert, K. A. Zvezdin, K. Yakushiji, H. Kubota, A. Fukushima, S. Yuasa, K. Nishimura, Y. Nagamine, H. Maehara, K. Tsunekawa, V. Cros, and J. Grollier, Sci. Rep. **3**, 1829 (2013).

[19] J. Dean, M. T. Bryan, T. Schrefl, D. A. Allwood, J. Appl. Phys. **109**, 023915 (2011).

[20] M. T. Bryan, J. Dean, and D. A. Allwood, Phys. Rev. B **85**, 144411 (2012).

[21] H. Sohn, M. E. Nowakowski, C. Y. Liang, J. L. Hockel, K. Wetzlar, S. Keller, B. M. McLellan, M. A. Marcus, A. Doran, A. Young, M. Kläui, G. P. Carman, J. Bokor, R. N. Candler, ACS Nano **9**, 4814 (2015).

[22] J.-M. Hu, T. Yang, K. Momeni, X. Cheng, L. Chen, S. Lei, S. Zhang, S. Trolier-McKinstry, V. Gopalan, G. P. Carman, C.-W. Nan, and L.-Q. Chen, Nano Lett. **16**, 2341 (2016).

[23] E. Mikheev, I. Stolichnov, E. De Ranieri, J. Wunderlich, H. J. Trodahl, A. W. Rushforth, S. W. E. Riester, R. P. Campion, K. W. Edmonds, B. L. Gallagher, and N. Setter, Phys. Rev. B **86**, 235130 (2012).

[24] J. H. Franken, Y. Yin, A. J. Schellekens, A. van den Brink, H. J. M. Swagten and B. Koopmans, Appl. Phys. Lett. **103**, 102411 (2013).

[25] N. Lei, T. Devolder, G. Agnus, P. Aubert, L. Daniel, J.-V. Kim, W. Zhao, T. Trypiniotis, R. P. Cowburn, C. Chappert, D. Ravelosona, and P. Lecoeur, Nat. Commun. **4**, 1378 (2013).

[26] E. De Ranieri, P. E. Roy, D. Fang, E. K. Vehsthedt, A. C. Irvine, D. Heiss, A. Casiraghi, R. P. Campion, B. L. Gallagher, T. Jungwirth, and J.Wunderlich, Nat. Mater. **12**, 808 (2013).

[27] B. Van de Wiele, L. Laurson, K. J. A. Franke, and S. van Dijken, Appl. Phys. Lett. **104**, 012401 (2014).

[28] K. J. A. Franke, B. Van de Wiele, Y. Shirahata, S. J. Hämäläinen, T. Taniyama, and S. van Dijken, Phys. Rev. X **5**, 011010 (2015).

[29] N. A. Pertsev, Appl. Phys. Lett. **102**, 112407 (2013).

[30] N. Tiercelin, Y. Dusch, A. Klimov, S. Giordano, V. Preobrazhensky, and P. Pernod, Appl. Phys. Lett. **99**, 192507 (2011).

[31] S. Giordano, Y.Dusch, N. Tiercelin, P. Pernod, and V. Preobrazhensky, Phys. Rev. B **85**, 155321 (2012).

[32] Y. Dusch, N. Tiercelin, A. Klimov, S. Giordano, V. Preobrazhensky, and P. Pernod, J. Appl. Phys. **113**, 17C719 (2013).

[33] S. Giordano, Y. Dusch, N. Tiercelin, P. Pernod, and V. Preobrazhensky, Eur. Phys. J. B **86**, 249 (2013).

[34] S. Giordano, Y. Dusch, N. Tiercelin, P. Pernod, and V. Preobrazhensky, J. Phys. D : Appl. Phys. **46**, 325002 (2013).

[35] N. Tiercelin, Y. Dusch, S. Giordano, A. Klimov, V. Preobrazhensky, and P. Pernod, *Strain Mediated Magnetoelectric Memory*, in *Nanomagnetic and Spintronic Devices for Energy-Efficient Memory and Computing*, eds. Supriyo Bandyopadhyay, Jayasimha Atulasimha (Wiley, 2016).

[36] A. K. Biswas, S. Bandyopadhyay, and J. Atulasimha, Appl. Phys. Lett. **104**, 232403 (2014).

[37] H. Ahmad, J. Atulasimha, and S. Bandyopadhyay, Sci. Rep. **5**, 18264 (2015).

[38] C.-Y. Liang, A. Sepulveda, S. Keller and G. P. Carman, J. Appl. Phys. **119**, 113903 (2016).

[39] T. Mathurin, S. Giordano, Y. Dusch, N. Tiercelin, P. Pernod, and V. Preobrazhensky, Appl. Phys. Lett. **108**, 082401 (2016).

[40] T. Mathurin, S. Giordano, Y. Dusch, N. Tiercelin, P. Pernod, and V. Preobrazhensky, Eur. Phys. J. B **89**, 169 (2016).

[41] T. Mathurin, S. Giordano, Y. Dusch, N. Tiercelin, P. Pernod, and V. Preobrazhensky, Phys. Rev. B. **95**, 140405(R) (2017).

[42] C.W. Nan, M.I. Bichurin, S. Dong et al. J. Appl. Phys. **103**, 31101 (2008).

[43] S. Giordano, M. Goueygou, N. Tiercelin, A. Talbi, P. Pernod, and V. Preobrazhensky, Int. J. Eng. Science **78**, 134 (2014).

[44] S. Giordano, Mech. Res. Comm. **55**, 18 (2016).

[45] S. Giordano, Mech. Mater. **105**, 16 (2017).

[46] N. L. Schryer, and L. R. Walker, J. Appl. Phys. **45**, 5406 (1974).

[47] F. Cayssol, D. Ravelosona, C. Chappert, J. Ferré, and J. P. Jamet, Phys. Rev. Lett. **92**, 107202 (2004).

[48] L. Landau and E. Lifshitz, Phys. Zeitsch. der Sow. **8**, 153 (1935).

[49] T. L. Gilbert, Phys. Rev. **100**, 1243 (1955) (abstract only) ; IEEE Trans. Mag. **40**, 3443 (2004).

[50] F. Wang, L. Luo, D. Zhou, X. Zhao, and H. Luo, Appl. Phys. Lett. **90**, 212903 (2007).

[51] N. A. Pertsev, Phys. Rev. B **78**, 212102 (2008).

[52] Y. Dusch, N. Tiercelin, A. Klimov, V. Rudenko, Y. Ignatov, S. Hage-Ali, P. Pernod, and V. Preobrazhensky, J. Appl. Phys. **109**, 07A720 (2011).